New System for Detecting Road Ice Formation

INVESTIGATION OF A NEW SYSTEM FOR THE DETECTION OF ROAD ICE FORMATION

Amedeo Troiano, Eros Pasero, Luca Mesin

Dipartimento di Elettronica, Politecnico di Torino, Torino, Italy

Address for correspondence:

Amedeo Troiano

Dipartimento di Elettronica, Politecnico di Torino; Corso Duca degli Abruzzi 24, Torino, 10129 ITALY

Tel. +39 011 5644103; Fax. +39 011 5644103; e-mail: amedeo.troiano@polito.it

ABSTRACT

The reliable detection of water and ice over road surfaces is an important issue in improving traffic safety and reducing costs for the maintenance of routs, especially during winter. A low cost capacitive sensor for the estimation of road conditions is studied. A simulation model was developed to investigate the capacitance of the sensor when air, water, or ice are covering its surface and to assess the effect of the variation of environmental temperature, or of the thickness of water or ice. An algorithm for the estimation of the state of the sensor (dry, wet, or icy) was developed based on the results of the simulations, which indicated that the time derivative of the estimated capacitance provided optimal information. Accuracy and reliability of the estimates provided by the sensor were assessed in laboratory experiments, placing more sensors in a climatic chamber and investigating the estimated state of the sensors and the timing of the identification of wet-icy or icy-wet transitions. Reliable estimates were obtained by all the sensors, with a dispersion of the transition times of the order of a few minutes. The sensor was also investigated in field. Two sensors (one of which was bituminized) were embedded in a road pavement to monitor continuously the road surface condition for a month. Both sensors provided indications in line with the environmental conditions, identifying properly the icy condition and indicating the wet state of the road both during rain and fog. Thus, the sensor is suggested as a feasible tool for monitoring road conditions to support information systems improving security and efficient maintenance of roads during winter.

Keywords: sensor, ice detection, road information

1. INTRODUCTION

The investigation of ice formation found important applications in different fields. An adequate assessment of the environmental conditions on road surfaces may significantly contribute to enhanced traffic safety, since corresponding decision made by administrators may be based on this information [1]. An important application is on the runway of airports, in order to improve safety during take off and landing of the aircrafts [1]. The accretion of ice is a common occurrence on the aircraft, due to the high flight speed associated to the humidity and low temperature in upper air. This is a critical issue since the aerodynamics of the aircraft change, and there is the risk that ice comes off during the flight, possibly striking and damaging the engine [2, 3, 4, 5, 6]. Investigation of ice formation on the seas is important to monitor iceberg formation and accretion [7, 8, 9, 10], and to prevent possible crashes with boats. Moreover, indication of the presence of ice on the walkways is useful to prevent people falls.

Different ice detection technologies were developed, depending on the application. Some techniques work putting a sensor in contact with the surface over which ice may form [3], others allow for a remote sensing [6, 9]. Different techniques may be further distinguished between those providing local information obtained from single point detectors [4] and those performing wide-area measurements [5]. Different kinds of sensors were developed exploiting different physical principles, e.g. concerning vibration [11, 12], electro-optics [13], fiber-optics [4, 14], radio frequency [15], micro-mechanics [16], ultrasounds [2, 17]), inductive [18] and capacitive [19] effects.

The reliable detection of water and ice is one of the main problems in the assessment of the environmental conditions on road surfaces. The investigation of road conditions is attracting increasing attention, as it may significantly contribute to improve traffic safety and to reduce costs of highway snow and ice control [20, 21]. Road Weather Information Systems (RWIS)

consist of specialized weather stations that provide information on road surface conditions and weather forecast. RWIS allows agencies to efficiently plan the maintenance of roads during winter, to reduce wear on the vehicle fleet, to decrease chemical, sand and salt usage, and to provide a better level of service by applying anti-icing practices. Three types of road weather information are important: atmospheric data (e.g. air temperature and humidity, visibility, wind speed and direction, precipitation type and rate, cloud cover, lightning, air quality), water level data (stream, river and lake levels near roads), and pavement data (temperature, freezing point, chemical concentration and pavement condition, e.g., dry, wet, or icy). Pavement data are typically used to forecast surface conditions and choose proper anti-icing procedures. Thus, one of the key objectives of modern RWIS is the detection of the presence of water, snow, ice and the beginning formation of ice [22].

An innovative ice sensor was introduced in [19]. The sensor detects water and ice on exposed surfaces, based on a capacitance measurement. This work is devoted to the investigation of the accuracy and reliability of the indication provided by this new ice detection system, using both a mathematical model for the simulation of the system and experimental results. The application of the sensor within an Airport Winter Information System (AWIS), which is a system supporting management and safety of a large airport during winter events [23], is discussed.

2. METHODS

2.1 Ice detection system

The ice detection system consists in a capacitance measurement [1, 19]. In general, the value of capacitance of the electrode assembly depends on the geometrical configuration and dimensions of the electrodes, and on the permittivity and thickness of the material placed between the electrodes.

The permittivity, in turn, depends on temperature and measurement frequency. The relation between the relative permittivity of water or ice, and the temperature and measurement frequency is shown in Figure 1. The relative permittivity of ice at approximately –1°C is substantially constant within a range from DC to about 1kHz, and decreases in the range of approximately 2kHz to several hundred kHz. On the other hand, the relative permittivity of water at approximately 1°C is substantially constant up to approximately 10^9Hz and decreases within the range from 10^9Hz to 10^{10}Hz. The relative permittivity of air can be assumed as low and constant for each frequency.

When measuring the capacitance, due to the confounding factors (e.g., thickness of water), it is not possible to distinguish reliably water and ice at low frequencies (lower than 1kHz), but only air can be identified; on the other hand, ice and air cannot be distinguished at high frequencies (between 100kHz and 1GHz), but it is possible to identify the presence of water using such a high frequency. Thus, it is possible to distinguish between water, ice and air by two capacitive measurements, at low and high frequencies [19].

Figure 1 about here

The currently available ice sensor is shown in Figure 2A. This device performs measurements at three different frequencies, at 200Hz, 500Hz, and 20MHz. The sensor system consists on a pair of concentric conductive electrodes (with geometry shown in Figure 2B and dimensions indicated in Figure 3B), which constitute the sensing device, a frequency generator and a charge detector. The sensor electrodes of the ice detector are directly connected to the capacitance measurement circuit, shown in Figure 2C. This circuitry is implemented on a printed circuit board (PCB) using commercial available low power components. The frequency generator is obtained by a reference voltage source V_R and a controllable switch

S_1 to provide different frequencies. The electrode assembly and the material placed over the sensor constitute the capacitor C_X. In the basic measurement circuit, the charge detector comprises only a reference capacitance C_S that is connected to the electrodes by closing the switch S_2.

Figure 2 about here

The charge Q_X stored in the electrode assembly is:

$$Q_X = C_X \cdot V_R \tag{1}$$

When the switch S_2 is closed, the charge stored in the electrode assembly is partially transferred to the detection capacitance:

$$Q_X = (C_S + C_X) \cdot V_S \tag{2}$$

Since the value of the sensor electrode is several orders of magnitude lower than C_S, nearly all charge stored in C_X is transferred to the detection capacitance:

$$Q_X = C_X \cdot V_R = C_S \cdot V_S \tag{3}$$

and therefore, measuring the voltage level V_S reached by the detection capacitance, the capacitor value of the electrode assembly can be calculated as:

$$C_X = C_S \frac{V_S}{V_R} \tag{4}$$

In order to increase accuracy in measuring the very small value of capacitance C_X, the sensor was charged n times and its charge was transferred n times to the reference capacitor before taking a measurement of V_S. Therefore the value of the capacitance of the sensor is given by

$$C_X = \frac{C_S}{n} \frac{V_S}{V_R} \tag{5}$$

At the end of the measurement process, C_S is discharged by closing the switch S_3.

In the currently available ice sensor, the reference voltage V_S is equal to 3V (tolerance of 0.2%), the value of the reference capacitance C_S is equal to 2.2nF (tolerance equal to 1%), and the number of times the reference capacitor is charged before taking a measurement is n=50. The voltage level V_S is first amplified by a factor 150 by an analog circuit and then sampled by the analog to digital converter (10 bit resolution) of a microcontroller (8051 core from Silicon Laboratories Inc), using a sampling frequency of 0.2Hz. The switches S_1, S_2, and S_3 are obtained using high-bandwidth FET transistors.

An automatic calibration procedure is included in the ice sensor to prevent error in the data due to parasitic capacitances [19]. Also the capacitance of the dry electrode, which is about 0.3pF (measured using a high-resolution RLC meter – Fluke PM 6306), is subtracted by the calibration procedure. The device also comprises an internal temperature sensor, to account for variations of the relative permittivity with temperature.

A layer 3 mm thick of Arnite was mounted over the sensor electrode, for protection purposes. Arnite was chosen because its dielectric constant is nearly constant (equal to 3.4) within the range of temperatures and measurement frequencies in which the sensor is used.

The ice detection system arrangement was inserted into a metallic box filled with resin, which protects the circuitry from infiltration of water or chemical agents. The only exposed parts are the Arnite covering the sensor (on the top) and the connector for the power supply of the circuitry and for the RS-485 communication protocol (on the bottom) used to connect the sensor to a data acquisition system. The acquisition system is used to collect data from more sensors and to send them to a computer for storing (C_X values at the three measurement frequencies and internal temperature) and to perform signal processing on the values of capacitance.

2.2 Mathematical model

The sensor was described using a multi-layer electrostatic model (at the maximum measurement frequency, the wave length of the electromagnetic field is more than two orders of magnitude greater than the dimensions of the sensor):

$$-\nabla \cdot (\underline{\underline{\varepsilon}} \nabla \varphi) = 0 \tag{6}$$

where φ is the potential (V) and $\underline{\underline{\varepsilon}}$ is the dielectric tensor (F/m). Two layers were included (see Figure 3A): a dielectric (e.g. the Arnite protecting the sensor) covering the electrodes and water or ice. Both layers were assumed to be isotropic and of constant thickness. For the first layer, a constant value of dielectric constant $\varepsilon_1 = 3.5$ was assumed. The relative permittivity of water ε_2 was modelled as:

$$\varepsilon_2(f) = \varepsilon_\infty + \frac{\varepsilon_s - \varepsilon_i}{1 + jf / f_1} + \frac{\varepsilon_i - \varepsilon_\infty}{1 + jf / f_2} \tag{7}$$

where all parameters (static permittivity ε_s, high frequency permittivity ε_∞, intermediate frequency dielectric constant ε_i, relaxation frequencies f_1 and f_2) are functions of temperature [24]. The relative permittivity of ice (again indicated with ε_2) was modelled as a Debye model [25]:

$$\varepsilon_2(f) = \varepsilon_\infty + \frac{\varepsilon_s - \varepsilon_\infty}{1 + j2\pi\tau f} \tag{8}$$

in which the static permittivity ε_s was 75, the high frequency permittivity ε_∞ was 3.2 and the relaxation time τ was dependent on temperature, assuming a linear variation between the values $1.4 \cdot 10^{-4}$ at -20°C and $2.5 \cdot 10^{-5}$ at 0°C [26]. Figure 1 shows the real part of the relative permittivity of pure water and ice for different temperatures.

Thus, the two layers were studied as different sub-domains in which Laplace equation $\Delta\varphi = 0$ was solved. Such sub-domains were coupled by the interface conditions between the

two layers requiring that the potential and the dielectric displacement $\vec{D} = \underline{\underline{\varepsilon}} \nabla \varphi$ were continuous crossing the interface.

As the electrodes are circular (see Figure 3A), the problem was considered symmetrical in cylindrical coordinates (ρ, θ, z). A mixed boundary value problem was studied, imposing opposite value of potential on the two electrodes and vanishing dielectric displacement on the other part of the boundary. Due to the cylindrical symmetry of the problem, the potential does not depend on the angle θ, but only on the radius ρ and on the depth within the layers z. The problem can be stated as follows:

$$\begin{cases} \Delta\varphi_1 = \dfrac{\partial^2 \varphi_1}{\partial \rho^2} + \dfrac{1}{\rho}\dfrac{\partial \varphi_1}{\partial \rho} + \dfrac{\partial^2 \varphi_1}{\partial z^2} = 0 & \rho > 0,\ 0 < z < z_I \\ \Delta\varphi_2 = \dfrac{\partial^2 \varphi_2}{\partial \rho^2} + \dfrac{1}{\rho}\dfrac{\partial \varphi_2}{\partial \rho} + \dfrac{\partial^2 \varphi_2}{\partial z^2} = 0 & \rho > 0,\ z_I < z < z_0 \\ \varphi_1\big|_{z_I^-} = \varphi_2\big|_{z_I^+} & \\ \varepsilon_1 \dfrac{\partial \varphi_1}{\partial z}\bigg|_{z_I^-} = \varepsilon_2 \dfrac{\partial \varphi_2}{\partial z}\bigg|_{z_I^+} & \\ \varphi = V_0 e^{j2\pi ft} & \rho \le \rho_0,\ z = 0 \\ \varphi = -V_0 e^{j2\pi ft} & \rho_{\text{int}} \le \rho \le \rho_{ext},\ z = 0 \\ \dfrac{\partial \varphi}{\partial \rho} = 0 & \rho = 0 \\ \dfrac{\partial \varphi}{\partial z} = 0 & \rho_0 < \rho < \rho_{\text{int}} \cup \rho > \rho_{ext},\ z = 0 \\ \dfrac{\partial \varphi}{\partial z} = 0 & z = z_0 \end{cases} \tag{9}$$

where ρ_0 is the radius of the internal electrode, ρ_{int} and ρ_{ext} are the internal and external radiuses defining the ring shape electrode, z_I is the depth of the interface between the two layers and z_0 is the total thickness of the domain (i.e., the sum of the thicknesses of the two layers; see Figure 3A). The last boundary condition in (9) was assumed in the case in which the second layer contains water, because the jump of dielectric constant between water and

the external air (with simulated relative permittivity 1) is very high, in the considered range of frequencies. When the second layer included ice and the considered frequency was high, the dielectric constants of ice and of the covering air are comparable. In such a case, a three layer model was simulated (with a straightforward generalization of the two layer model described above) including air over the second layer. The estimated capacitance is a monotonic increasing function of the thickness of such a third layer, but saturates within a few simulated mm of air; thus, the simulated thickness of air was chosen to be 25mm, assuring that the capacitance curve saturated.

The mathematical problem (9) was solved using finite difference method. The domain was limited imposing a maximum radius of 30mm. Homogeneous Neumann condition $\frac{\partial \varphi}{\partial \rho} = 0$ was imposed on such a new boundary.

A non-uniform discretization of the domain was used, with increasing resolution close to the electrodes and to the interface (Figure 3B). Specifically, the sampling step of the radius $\Delta\rho$ was 1% of the maximum radius (30mm) close to the electrodes and 3% of the maximum radius otherwise; in the case of a two layer model, the discretization step of the depth variable Δz was 1% of the sum of the thicknesses of the two layers z_0 close to the electrode surface $z = 0$ and to the interface $z = z_I$, and 3% otherwise. When a third layer was included, the same sampling of the first two layers was used, but the sampling step in the third layer was about 3% of the total thickness of the simulated domain.

Derivatives were discretized with a second order approximation both within the domain and on the boundary:

$$\left.\frac{\partial u}{\partial x}\right|_{x_0} \cong a\,u(x_0) + b\,u(x_0 + h_1) + c\,u(x_0 + h_2);\ \text{where } a = -\frac{h_1 + h_2}{h_1 h_2}, b = -\frac{h_2}{h_1(h_1 - h_2)}, c = \frac{h_1}{h_2(h_1 - h_2)}$$
$$\left.\frac{\partial^2 u}{\partial x^2}\right|_{x_0} \cong a\,u(x_0) + b\,u(x_0 + h_1) + c\,u(x_0 + h_2);\ \text{where } a = \frac{2}{h_1 h_2}, b = \frac{2}{h_1(h_1 - h_2)}, c = -\frac{2}{h_2(h_1 - h_2)} \quad (10)$$

where h_1 and h_2 have the same sign when the considered point x_0 is on a boundary or different signs when x_0 is within the domain. A linear system of algebraic equations was obtained after discretization. The potential was estimated inverting such a system using Gauss elimination method.

Given the potential, the charge q over the internal electrode (which is the same except for the sign as that over the external ring electrode) was estimated as:

$$q = \Re\left[\int_{\rho\le\rho_0, z=0} \vec{D}\cdot\hat{n}dS\right] = 2\pi\varepsilon_1 \int_0^{\rho_0} r\frac{\partial\Re[\varphi]}{\partial r}dr \tag{11}$$

Finally, the capacitance was obtained as:

$$C = \frac{q}{2V_0} \tag{12}$$

Figure 3 about here

2.3 Experiments

The reliability of the estimates provided by the ice sensor was investigated during laboratory and in field experiments.

Laboratory tests were performed applying the same environmental conditions to more ice sensors and evaluating the dispersion of the time instants in which phase changes of water were detected. Nine ice sensors were placed at the same time in a climatic chamber (Angelantoni - Challenge 250; temperature range for climatic test from -40°C to +180°C). At the beginning of the experiment, sensors were placed in the climatic chamber at ambient conditions, with a temperature of 25°C and humidity of 50%, for approximately 10 minutes in order to wait that the indications of the sensor became stationary. Then, 1 mm of tap water

was placed over each sensor. Sensors were left in ambient conditions for 10 minutes. Then, the climatic chamber was arranged to reach -20°C with a temperature gradient of -1°C per minute. During this period, water placed over sensors froze. The climatic chamber kept the temperature of -20°C for approximately 10 minutes and then it was arranged to reach 25°C with a temperature gradient of 1°C per minute. During this period, the ice formed over the sensors melt. The climatic chamber kept the temperature of 25°C for approximately 10 minutes. Then each sensor was dried. Data were acquired for additional 10 minutes, with a temperature of 25°C and humidity of 50%. The experiment was repeated in three different days, in order to investigate the repeatability of the values of capacitance and the reliability of the sensor.

In field tests were performed on two sensors, one standard sensor and a sensor covered by bitumen (bituminized sensor). The sensors were embedded in a secondary street close to the runway at the Turin-Caselle airport. Moreover, a complete weather station (PCE Group – PCE FWS-20) was placed close to the sensors to monitor meteorological variables, such as ambient humidity, temperature, pressure, velocity and direction of the wind, and quantity of rain falls. The in field test was performed over a period of 36 days.

2.4 Signal processing

In order to discriminate between different states of the sensor surface (dry, wet, or icy), the values of capacitance obtained at the three measurement frequencies were digitally processed using an innovative algorithm. Data were digitally low-pass filtered (cut-off frequency of 0.002Hz, 100^{th} order causal FIR filter) in order to reduce high frequency variations and instrumentation noise. Since jumps in the values of capacitance were associated to a state variation of the sensor (dry-wet, wet-icy, icy-wet, and wet-dry), a first-order derivative was computed on the filtered data in order to emphasize these jumps. A jump was considered

significant if the first-order derivative of the capacitance was higher than a threshold value estimated during the calibration. The algorithm identified the changes of the phase over the sensor based on the jumps on the first-order derivative of the values of capacitance estimated at the low and high measurement frequencies. Data from the intermediate frequency were not used in this work. The following 4 cases were considered.

1. Concurrent positive jumps at high and low measurement frequency indicates the transition from the state condition dry to wet.
2. Negative jump at high measurement frequency and no jump at low measurement frequency indicate the variation from wet to icy.
3. Positive jump at high measurement frequency and no jump at low measurement frequency indicate the transition from icy to wet.
4. Concurrent negative jumps at high and low measurement frequency indicates the change from wet to dry.

When none of the above conditions was satisfied, the state of the sensor was considered steady.

Capacitances and time instants of state transitions obtained for each sensor during the experiments were then compared in order to study the repeatability of the measures.

3. RESULTS

3.1 Validation of the mathematical model of the sensor

The mathematical model was validated based on both analytical and experimental data. Changing the boundary conditions of the model, it was possible to simulate a capacitor with parallel planar plates with a layer of dielectric covering the plates (with relative permittivity ε_1) and another internal layer (with relative permittivity ε_2). The analytical solution is:

$$C = \varepsilon_0 \frac{\varepsilon_1 \varepsilon_2}{\varepsilon_1 z_1 + \varepsilon_2 \frac{z_2}{2}} S \quad (13)$$

where z_1 is the thickness of the layers close to the plates, z_2 is the thickness of the internal layer, and S is the area of the plates. The relative error between the analytical and simulated solutions at different thickness of the internal layer was lower than 1.5%.

Simulated and experimental values of capacitance were compared. Representative results are shown in Figure 4A (simulations) and in Figure 5A (experiments). Results of simulations and experiments are similar, when considering that the capacitance of the dry electrode, subtracted by the calibration of the sensors, is about 0.3pF.

3.2 Simulation results

Simulated values of capacitance obtained using the mathematical model at different measurement frequencies, simulating the same environmental conditions of the experiment are shown in Figure 4A. Variations of the value of capacitance in different states of the sensor are clearly visible. During the dry and wet state of the sensor, the values of capacitance at high, medium, and low frequency were close to 0.3pF and 0.6pF, respectively. There was no distinction between different measurement frequencies, reflecting the constant value of relative permittivity of air and water in the considered range of frequency (Figure 1A). During the icy state of the sensors, the value of capacitance at high frequency was close to 0.45pF, whereas at medium and low frequency it was close to 0.6pF. Thus, there was an evident difference of the capacitance between the different frequencies, reflecting the variation of the permittivity of ice shown in Figure 1B. The value of capacitance obtained using the mathematical model simulating different thicknesses of water, from 0 (dry sensor) to 10mm, are shown in Figure 4B (temperature of 25°C and measurement frequency of 20MHz, but equivalent results are obtained for lower frequencies). The value of capacitance

rose slightly increasing the thickness of water over the sensor. Simulated values of capacitance for different thickness of ice are also shown in Figure 4B (temperature of -10°C and measurement frequency of 200Hz and 20MHz). Also increasing the thickness of ice formed over the sensor the values of capacitance rise. Simulated values of capacitance obtained for different measurement frequencies of water and ice are shown in Figure 4C (thickness of 1mm and a temperature of 25°C for water and -10°C for ice). Increasing the measurement frequency, the value of capacitance decreased, following the same trend of the relative permittivity.

Figure 4 about here

3.3 Experimental results

Values of capacitance (raw data) obtained from a sensor during the first experiment at different measurement frequencies are shown in Figure 5A. Variations of the values of capacitance in different states of the sensors are clearly visible. During the dry state, the values of capacitance are close to zero, due to the calibration procedure. During the wet state, the values of capacitance at high, medium, and low frequencies are close to 0.3pF, so that there is no distinction between different measurement frequencies. During the icy state, the values of capacitance at high frequency are close to 0.15pF while at medium and low frequency are close to 0.3pF, so that the value of capacitance can be easily distinguished for different measurement frequencies. Low-pass filtered values of capacitance are shown in Figure 5B. First-order derivative of the values of capacitance are shown in Figure 5C (below). Peaks are clearly visible in correspondence to a variation of the state of the sensor.

States of the sensor revealed by the algorithm described in Section 2.4 are shown in Figure 5C (above). The estimated states agreed with the observed state of the sensor (Figure 5A).

Figure 5 about here

Values of capacitance (raw data) obtained for each sensor during the first experiment (high and low measurement frequencies) are shown in Figure 6A. Differences among different sensors are visible, due to manufacturing tolerances and to low precision in controlling the thickness of the water layer. Internal temperature of the climatic chamber during the first experiment is shown in Figure 6B as measured by the internal temperature sensor of the ice detection system. The state condition detected by such a sensor is also shown. The wet-icy transition is identified at about -7°C, whereas the icy-wet transition is identified when the internal temperature is about 0°C. During the dry and wet states, the capacitance of the sensor at high and low measurement frequencies is quite similar, while during the icy state of the sensor there is a clear distinction between the values of capacitance obtained at the two measurement frequencies. Time instants of state transitions estimated for each sensor during the three experiments are shown in Figure 6C. The standard deviations of the time instants of the state transitions wet-icy and icy-wet estimated for each sensor are shown in Figure 6D (state transitions dry-wet and wet-dry were not considered since the sensors were wetting and drying by the user). In the three experiments, the standard deviation obtained for the state transition wet-icy is larger than that obtained for the state transition icy-wet. Moreover, there is no relevant difference between the standard deviation values obtained in the same state transitions for three experiments.

Figure 6 about here

Values of capacitance (raw data) obtained for the standard and bituminized sensors (high and low measurement frequencies) during the in field test at the Turin-Caselle airport, over the period 12/01/2010 – 17/02/2010, are shown in Figure 7A and 7B, respectively. States of the standard and bituminized sensors revealed by the algorithm are shown in Figure 7C. Meteorological data obtained by the weather station are shown in Figure 7D (quantity of rain falls), 7E (air humidity) and 7F (ambient temperature). During the test period, both sensors revealed different road surface conditions (dry, wet, and icy). A wet road surface condition was obtained during both rainy and foggy days.

Figure 7 about here

4. DISCUSSION AND CONCLUSIONS

This paper investigates the performance of a system which can be embedded in a road pavement to monitor continuously the road surface condition. The sensor is based on a multi-frequency measurement of capacitance and houses a cheap and efficient technology [1] to identify the presence of water or ice on the road. The sensor was investigated both with a simulation model and with experiments (in laboratory and in field conditions).

4.1 Simulations

Simulations provided a quantitative indication of the capacitance of the system according to the substance covering the sensor surface (air, water, or ice) as a function of the thickness of the layer of such a material, the temperature, and the measuring frequency. The capacitance of the simulated model is largely affected by the presence of water on the surface of the

sensor, so that a thin layer formed over it due to rain or moisture condensation can be identified. A variation of the thickness of the layer of water or ice covering the sensor or a variation of temperature does not affect deeply the value of capacitance. Therefore simulations suggest that an increasing or decreasing quantity of water or ice covering the sensor or a variation of the environmental temperature determine only smooth variations of the value of capacitance. On the other hand, abrupt variations of the capacitance on specific frequencies may indicate only a change of state of the sensor (dry, wet, or icy). Thus, the state of the sensor was estimated based on the time derivative of the measured capacitance (appropriately smoothed in order to eliminate spurious noise present on experimental data) instead of using a set of thresholds to be compared to the measurements, as previously proposed [1]. This method improved the reliability and stability of the estimates (results not shown).

4.2 Experiments

More sensors were investigated on the same laboratory conditions in order to assess the dispersion of the times in which transitions between wet and icy states were. Differences of the estimated times of transition were of the order of a few minutes, which is related to the spatial heterogeneity of the icing and melting processes. A higher dispersion was found in the case of wet-icy transition with respect to the icy-wet one. Indeed, water started freezing from the surface proceeding downward, so that a small difference in the thickness of the layer of water could determine a spread of the delays of different sensors in the identification of the presence of ice. On the other hand, the melting process started at the sensor surface (probably due to low energy dispersions from the device).

The wet-icy transition was detected at lower temperatures with respect to the icy-wet transition in the laboratory experiments. This is probably due to the freezing and melting

processes described above, but also to the higher value of specific heat for water (about 4000 J kg^{-1} K^{-1}) with respect to ice (about 2000 J kg^{-1} K^{-1}), which determines a higher time to cool water than that needed to warm ice, keeping constant the magnitude of the temperature gradients imposed by the climatic chamber.

In field experiments were performed over a 36 days period for two sensors, one of which was covered by bitumen. Equivalent precision on the identification of wet conditions were obtained. The wet condition after raining lasted a bit longer for the bituminized sensor, probably due to the porosity of bitumen which determines a delayed drying with respect to the not bituminized sensor. Wet condition was identified also in the case of foggy weather, confirming that even a slow condensation of water over the sensor surface is associated to a jump in the value of capacitance which may be easily identified.

4.3 Limitations and future works

The measured value of capacitance also depends on possible contaminations (e.g. dirt, fuel or salt) present in the water covering the sensor. For this reason, a salinity sensor was included in the system proposed in [1]. Future work will be focused on the assessment of the effect of salt concentration of water on the indication of the considered sensor. The effect of water concentration on its permittivity will be included in the simulation model and experiments will be performed with water with different concentration of salt. These results should improve the estimates of the state of the sensor (compensating for the effect of salt concentration) and could possibly provide an indication of the concentration of salt in the water covering the sensor surface.

4.4 Applications

Data from the sensor can be transmitted (i.e., by GPRS or UMTS) to a central database which may integrate them with other meteorological variables (air humidity and temperature, rain) for forecast purposes. This system was developed within the project Airport Winter Information System (AWIS), with the goal to improve the security of a large airport, especially during winter emergencies. Important problems to be faced in these conditions are the security of the user, the accessibility of the runway (delays, closure), the corrosion of maintenance vehicles, aircrafts, and runway surfaces due to treatment with de-icing substances, the prevision of surface conditions in order to organize maintenance activities just in time, and the reliability of the control process of the surface of the runway. These problems are very similar to those faced by a Road Winter Information System (RWIS), where the same technology investigated in this paper may be applied.

4.5 Conclusions

A low cost capacitive sensor for the estimation of road condition is discussed. Performances of the sensor were investigated in simulations, laboratory and in field experiments. The sensor may find applications in monitoring road conditions to support information systems assuring security and efficient maintenance of roads or airports during winter.

Acknowledgements

This work was sponsored by the national project AWIS (Airport Winter Information System), funded by Piedmont Authority, Italy.

REFERENCES

[1] Meindl T., Moniaci W., Pasero E., Riccardi. M., An Embedded Hardware-Software System to Detect and Foresee Road Ice Formation, Proceeding of International Joint Conference on Neural Networks (IJCNN), Vancouver, Canada, 2006.

[2] Gao H., Rose J.L., Ice detection and classification on an aircraft wing with ultrasonic shear horizontal guided waves, IEEE Transactions on Ultrasonics, Ferroelectrics and Frequency Control, vol. 56(2), pp. 334 – 344, 2009.

[3] Roy S., Izad A., DeAnna R.G., Mehregany M., Smart ice detection systems based on resonant piezoelectric transducers, Sensors and Actuators A, vol. 69, pp. 243 – 250, 1998.

[4] Wei L., Jie Z., Lin Y., Hong Z., A Fiber-Optic Solution to Aircraft Icing Detection and Measurement Problem, Proceedings of International Conference on Information Technology and Computer Science (ITCS), Kiev, Ukraine, 2009.

[5] Bassey C.E., Simpson G.R., Aircraft Ice Detection using Time Domain Reflectometry with Coplanar Sensors, Proceedings of IEEE Aerospace Conference, Big Sky, Montana, USA, 2007.

[6] Pitertsev A.A., Yanovsky F.J., Polarimetric approach to detection of probable aircraft icing zones. Icing detection algorithms, Proceedings of European Radar Conference (EuRAD), Munich, Germany, 2007.

[7] Kawano K., Kudoh J., Four-dimensional histogram method for sea ice detection using NOAA AVHRR images, Proceedings of IEEE International Geoscience And Remote Sensing Symposium (IGARSS), Toulouse, France, 2003.

[8] Ezraty R., New-ice detection using microwave sensors. Proceedings of IEEE International Geoscience And Remote Sensing Symposium (IGARSS), Toulouse, France, 2003.

[9] Wang M., Shi W., Detection of Ice and Mixed Ice–Water Pixels for MODIS Ocean Color Data Processing, IEEE Transactions on Geoscience and Remote Sensing, vol. 47(8), pp. 2510 – 2518, 2009.

[10] Muramoto K.I., Saito H., Matsuura K., Yamanouchi T., Cloud and ice detection using NOAA/AVHRR data, Proceedings of IEEE International Geoscience and Remote Sensing Symposium (IGARSS), 1997.

[11] Daniels J., Ice detecting system, U.S. Patent 4775118, Oct. 4, 1988.

[12] Barre C., Lapeyronnie D., Salaun G., Ice detection assembly installed on an aircraft, U.S. Patent 7000871, Feb. 21, 2006.

[13] Anderson M., Electro-optic ice detection device, U.S. Patent 6425286, Jul. 30, 2002.

[14] Kim J.J., Fiber optic ice detector, U.S. Patent 5748091, May 5, 1998.

[15] Abaunza J.T., Aircraft icing sensors, U.S. Patent 5772153, Jul. 30, 1998.

[16] DeAnna R., Ice detection sensor, U.S. Patent 5886256, Mar. 23, 1999.

[17] Rose J.L., Pilarski A.B., Hammer J.M., Peterson M.T., Readio P.O., Contaminant detection system, U.S. Patent 5629485, May 13, 1997.

[18] Lee H., Seegmiller B., Ice detector and deicing fluid effectiveness monitoring system, U.S. Patent 5523959, Jun. 4, 1996.

[19] Pasero E., Riccardi M., Meindl T., Multi-frequency capacitive measurement device and a method of operating the same, U.S. Patent 0192568, Aug. 31, 2006.

[20] Boselly S.E., Benefit-Cost Assessment of the Utility of Road Weather Information Systems for Snow and Ice Control, Transportation Research Record, vol. 1352, pp. 75 – 82, 1992.

[21] Thornes J.E., Cost-effective snow and ice control for the 1990s, Transportation Research Record, vol. 1387, pp. 185 – 190, 1993.

[22] Lee N.S.T., Karimi H.A., Krakiwsky E.J., Road information systems: Impact of geographic information Systems Technology to Automatic Vehicle navigation and guidance, Proceeding of Vehicle Navigation and Information Systems Conference, Canada, 1989.

[23] Pasero E., Moniaci W., Raimondo G., AWIS: an Airport Winter Information System, Proceedings of XIV Standing International Road Weather Commission (SIRWEC), Prague, Czech Republic, 2008.

[24] Meissner T., Wentz F.J., The Complex Dielectric Constant of Pure and Sea Water from Microwave Satellite Observations. IEEE Transactions on Geoscience and Remote Sensing, vol. 42(9), pp. 1836 – 1849, 2004.

[25] Herique A., Kofman W., Determination of the ice dielectric permittivity using the data of the test in Antarctica of the Ground – Penetrating Radar for Mars ’98 mission, IEEE Transactions on Geoscience and Remote Sensing, vol. 35(5), pp. 1338 – 1349, 1997.

[26] Petrenko V.F., Whitworth R.W., Physics of ice, Oxford University Press Inc., New York, 1999.

BIOGRAPHIES

Amedeo Troiano graduated in 2006 and received the Ph.D. in 2010 in Electronics Engineering from Politecnico di Torino, Italy. Since 2010, he is a Fellow at the Neuronica Laboratory of the Department of Electronics, Politecnico di Torino. His research interests include the design of analog and digital electronic systems, hardware/software co-design, and intelligent sensor systems.

Eros Pasero graduated in 1980 in Electronics Engineering from Politecnico di Torino, Italy. From 1987 to 1990 he was Associate Professor of Electronics with the II University of Roma. Since 1991 he is Associate Professor of Electronics at Politecnico di Torino, where he is managing the Neuronica Laboratory of the Department of Electronics, Politecnico di Torino. His current research involves neural networks modelling and simulation and hardware implementations.

Luca Mesin graduated in Electronics Engineering in 1999 and received the Ph.D. in Applied Mathematics in 2003 from Politecnico di Torino, Italy. From 2003 to 2008 he was a Fellow of the Laboratory for Neuromuscular System Engineering of the Department of Electronics, Politecnico di Torino. Since 2008, he is Assistant Professor in Biomedical Engineering at the Department of Electronics, Politecnico di Torino. His main research activities are in the fields of signal processing and mathematical modelling.

FIGURE CAPTIONS

Figure 1: Relative permittivity of water as a function of temperature and measurement frequency. (A) Water at temperature higher than 0°C. (B) Ice at temperature lower than -1°C.

Figure 2: The ice sensor. (A) Picture of the ice sensor. (B) Picture of the concentric conductive electrodes. (C) Schematic layout of the capacitive measurement circuit. The charge detector includes the capacitor C_S, while the voltage V_S is converted by the digital-to-analog converter in order to calculate the relative permittivity. C_X indicates the sense electrode. The reference voltage source V_R together with the controllable switch S_1 achieves the frequency generator. The controllable switch S_2 connects the capacitances C_S and C_X for the following measuring phase. At the end of the measurement process, C_S is discharged by closing the controllable switch S_3.

Figure 3: Simulation model. (A) Geometry of the electrode assembly and representation of the two simulated layers. (B) Example of simulation of the potential in steady condition in the two layers, indicating the non uniform discretization of the domain.

Figure 4: Simulation results. (A) Simulated values of capacitance obtained using the mathematical model for different states of the sensors at different temperatures and measurement frequencies. Simulated temperature used in the mathematical model is also shown. (B) Simulated values of capacitance for different thicknesses of water or ice (temperature of 25°C for water and -10°C for ice). (C) Simulated values of capacitance at different measurement frequencies (thickness of 1mm, and a temperature of 25°C for water and -10°C for ice).

Figure 5: Signal processing algorithm applied to the experimental data. (A) Values of capacitance (raw data) obtained for the sensor number 8 during the first experiment at different measurement frequencies. (B) Low pass filtered values of capacitance obtained from the raw data. (C) States of the sensor revealed by the algorithm (above). First-order derivative of the capacitance obtained from the low pass filtered data (below).

Figure 6: Statistical analysis of the laboratory data. (A) Values of capacitance (raw data) obtained for each sensor during the first experiment. (B) Internal temperature of the climatic chamber during the first experiment with the indication of the state condition detected by a sensor. (C) Time instants of state transitions estimated for each sensor during three different experiments. (D) Standard deviations of time instants of state transitions wet-icy and icy-wet estimated for each sensor during three different experiments.

Figure 7: In field results obtained from different sensors placed at the Turin-Caselle airport over the period 12/01/2010 – 17/02/2010. Values of capacitance (raw data) obtained for a standard sensor (A) and for a bituminized sensor (B). (C) States of the standard and bituminized sensors revealed by the algorithm. (D) Quantity of rain falls. (E) Ambient humidity. (F) Ambient temperature.

Figure 1

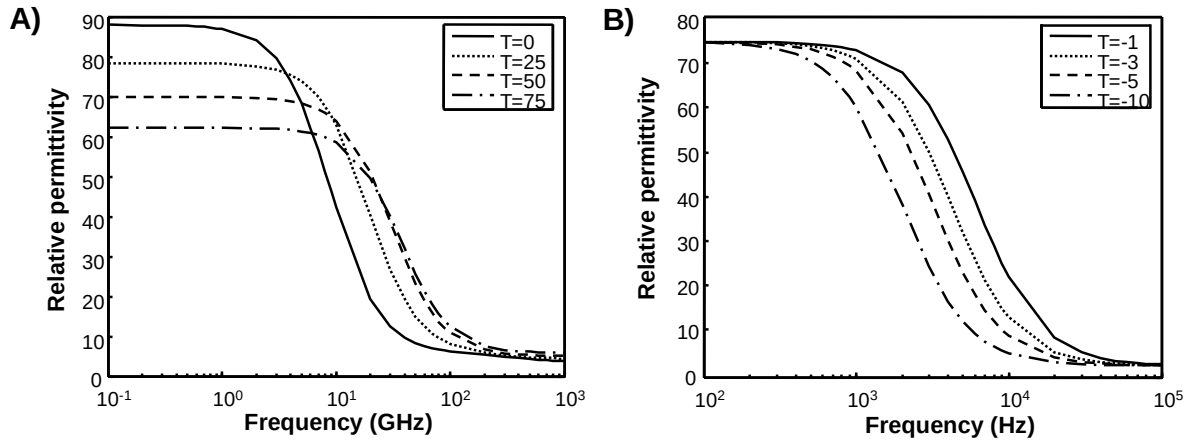
A)
Relative permittivity
Frequency (GHz)
T=0
T=25
T=50
T=75
B)
Relative permittivity
Frequency (Hz)
T=-1
T=-3
T=-5
T=-10

Figure 2

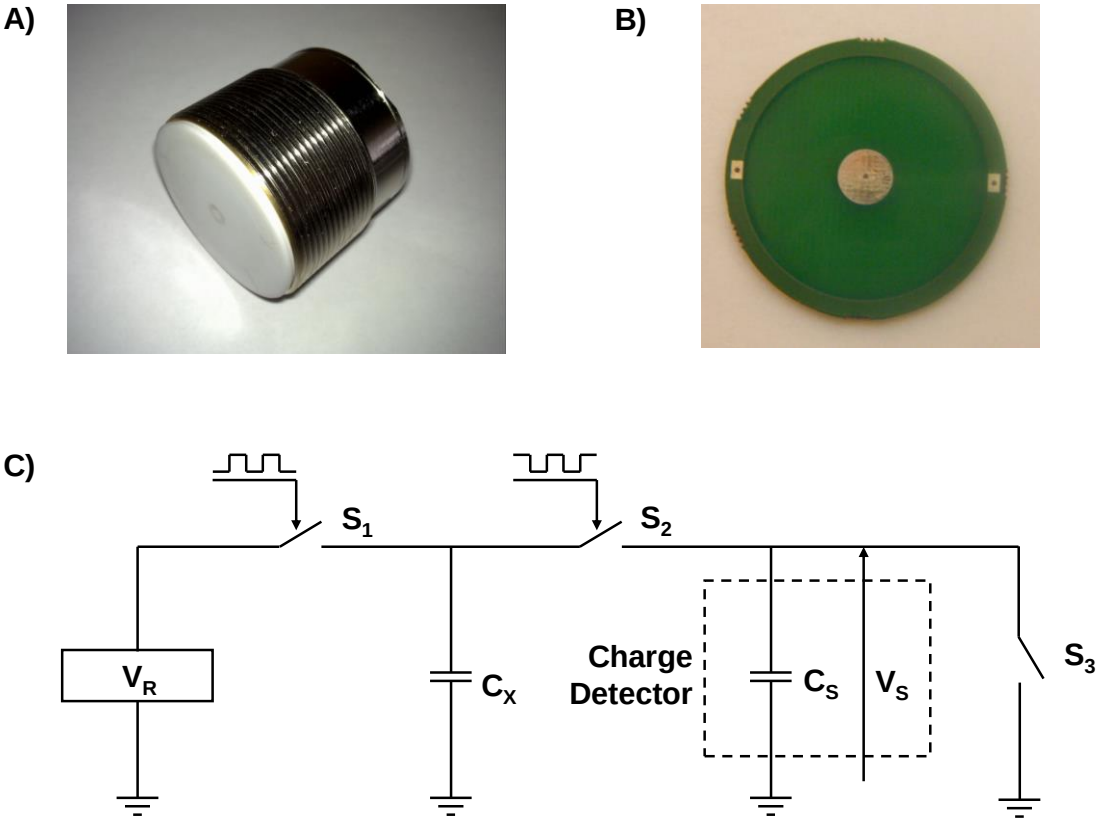

Figure 3

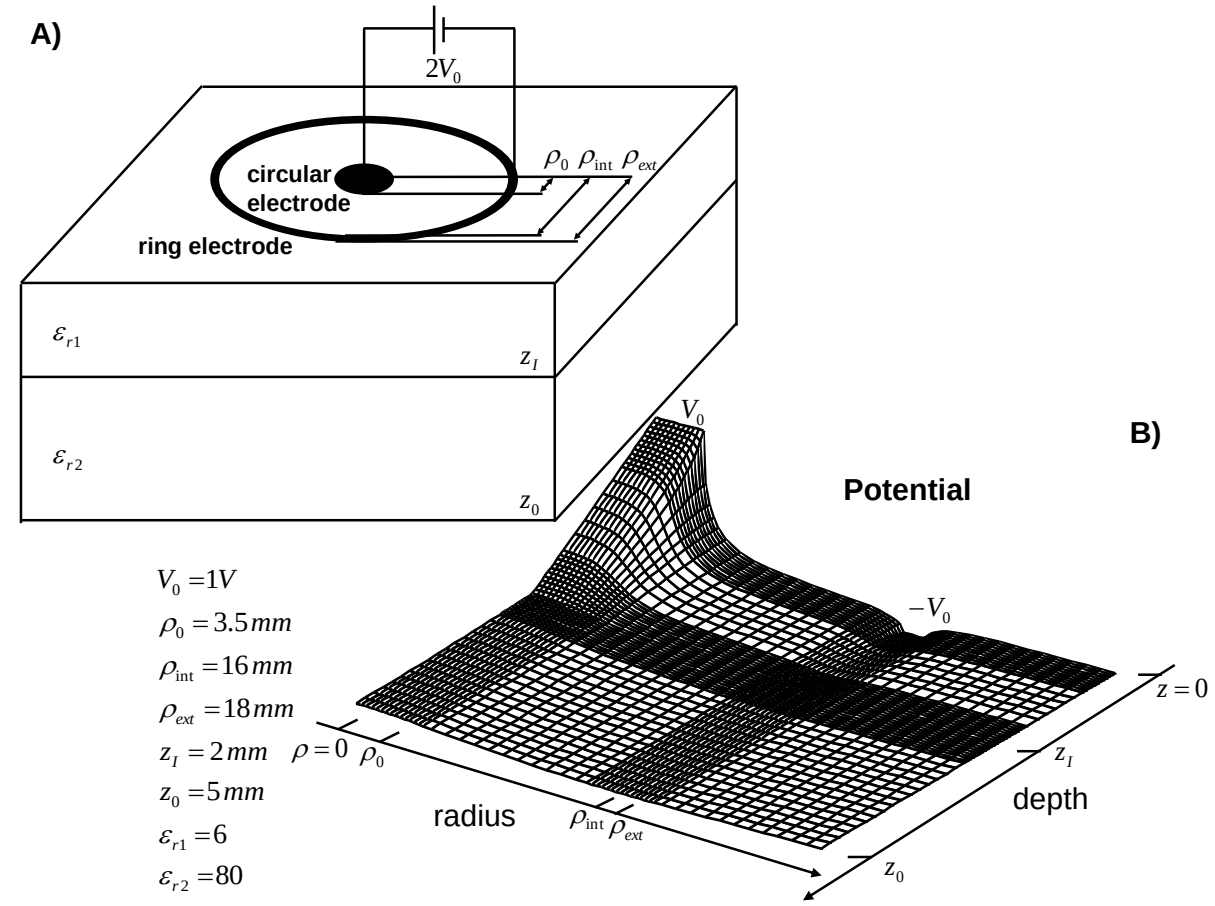
A)
$2V_0$
circular electrode
ring electrode
ρ_0 ρ_{int} ρ_{ext}
ε_{r1}
z_I
ε_{r2}
z_0
B)
Potential
V_0
$-V_0$
$V_0 = 1V$
$\rho_0 = 3.5mm$
$\rho_{\text{int}} = 16mm$
$\rho_{ext} = 18mm$
$z_I = 2mm$
$z_0 = 5mm$
$\varepsilon_{r1} = 6$
$\varepsilon_{r2} = 80$
$\rho = 0$ ρ_0
radius
ρ_{int} ρ_{ext}
$z = 0$
z_I
depth
z_0

Figure 4

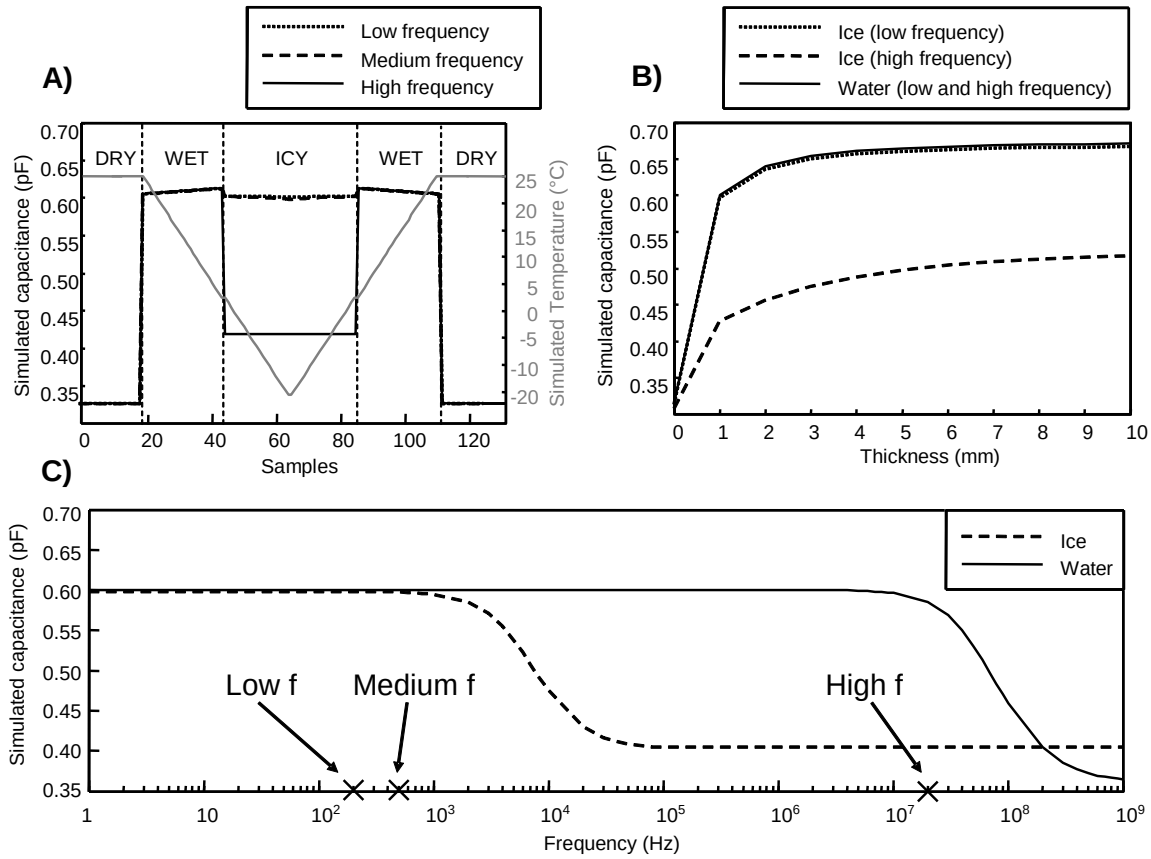
A)
Low frequency
Medium frequency
High frequency
DRY
WET
ICY
WET
DRY
Simulated capacitance (pF)
Simulated Temperature (°C)
Samples
B)
Ice (low frequency)
Ice (high frequency)
Water (low and high frequency)
Simulated capacitance (pF)
Thickness (mm)
C)
Ice
Water
Low f
Medium f
High f
Simulated capacitance (pF)
Frequency (Hz)

Figure 5

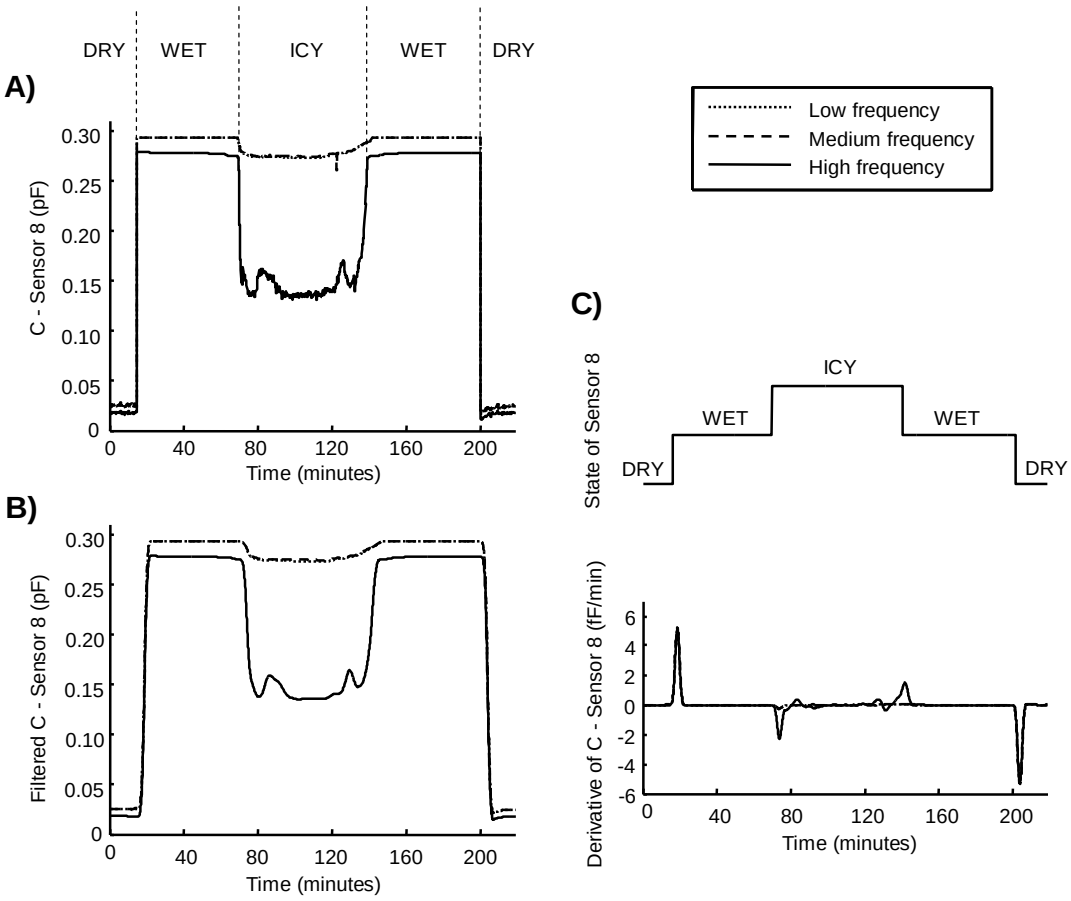
A)
DRY
WET
ICY
WET
DRY
C - Sensor 8 (pF)
0.30
0.25
0.20
0.15
0.10
0.05
0
0
40
80
120
160
200
Time (minutes)
Low frequency
Medium frequency
High frequency
B)
Filtered C - Sensor 8 (pF)
0.30
0.25
0.20
0.15
0.10
0.05
0
0
40
80
120
160
200
Time (minutes)
C)
State of Sensor 8
ICY
WET
WET
DRY
DRY
Derivative of C - Sensor 8 (fF/min)
6
4
2
0
-2
-4
-6
0
40
80
120
160
200
Time (minutes)

Figure 6

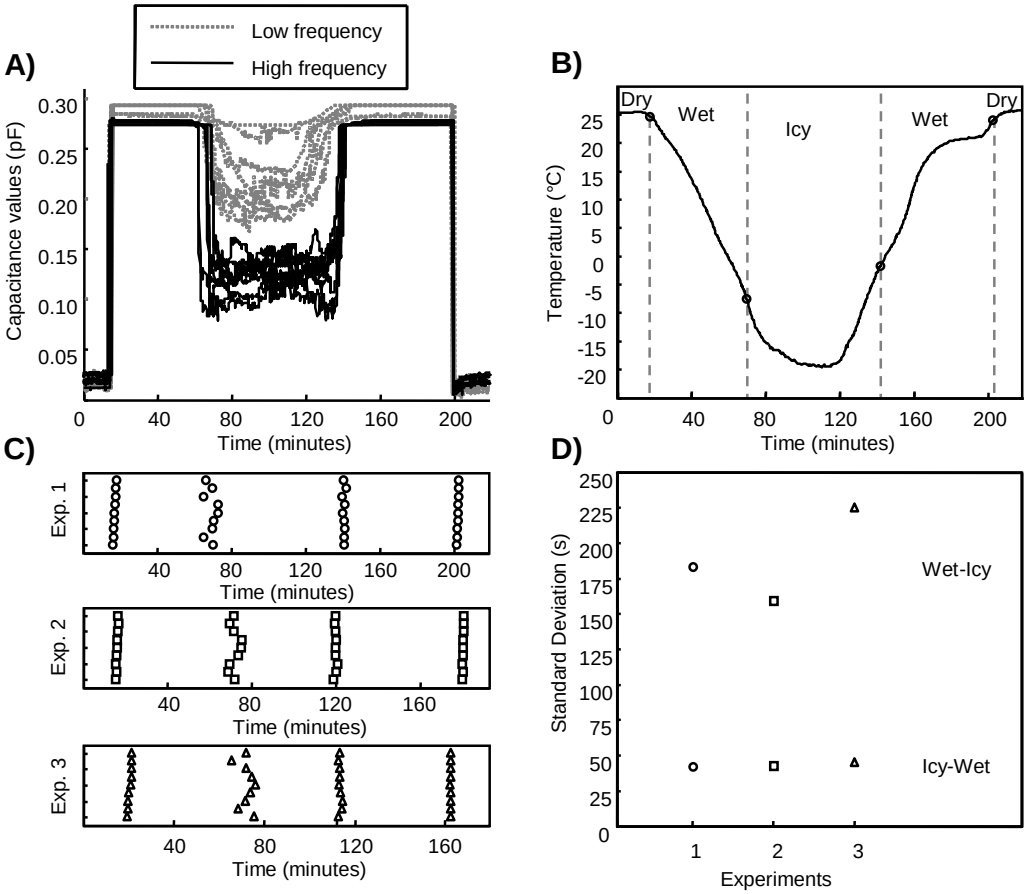
A)
Low frequency
High frequency
Capacitance values (pF)
Time (minutes)
B)
Dry
Wet
Icy
Wet
Dry
Temperature (°C)
Time (minutes)
C)
Exp. 1
Exp. 2
Exp. 3
Time (minutes)
D)
Standard Deviation (s)
Wet-Icy
Icy-Wet
Experiments

Figure 7

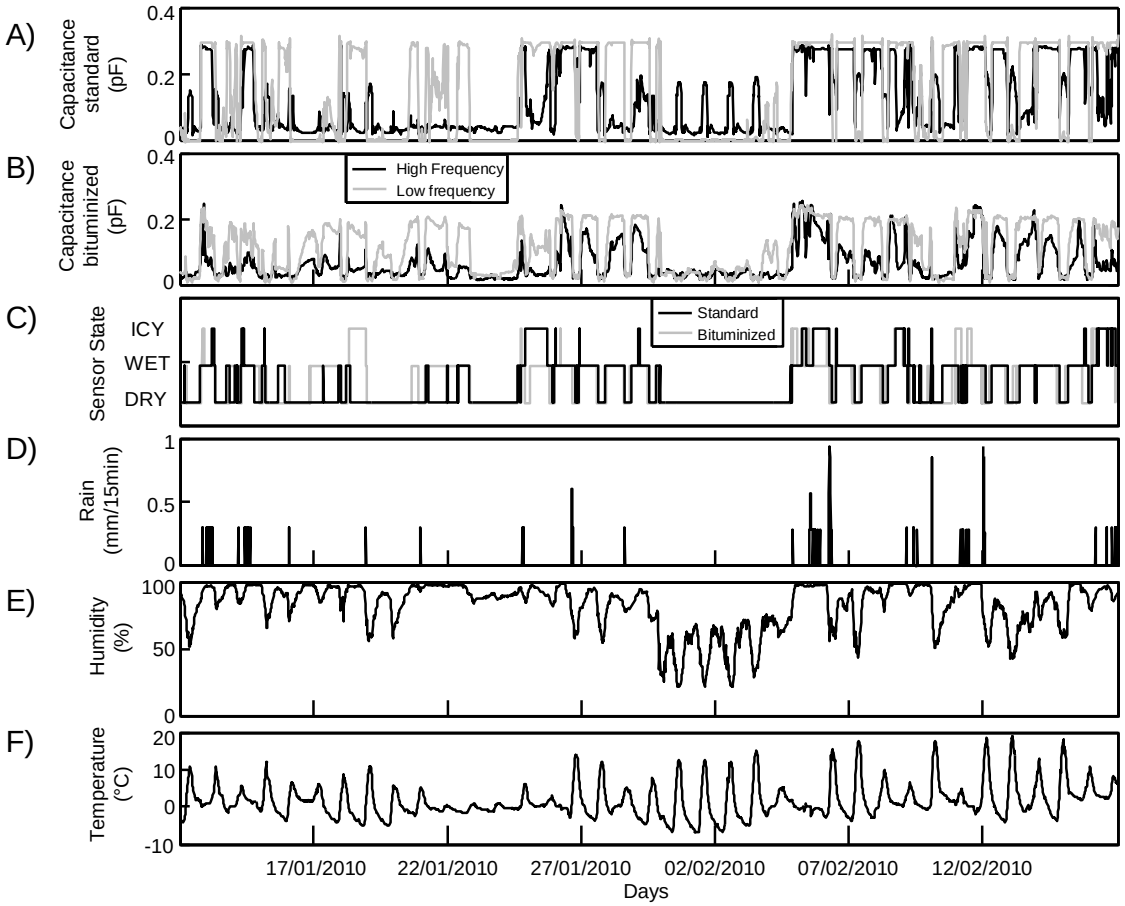
A)
Capacitance standard (pF)
0.4
0.2
0
B)
Capacitance bituminized (pF)
High Frequency
Low frequency
C)
Sensor State
ICY
WET
DRY
Standard
Bituminized
D)
Rain (mm/15min)
1
0.5
E)
Humidity (%)
100
50
F)
Temperature (°C)
20
10
-10
17/01/2010
22/01/2010
27/01/2010
02/02/2010
07/02/2010
12/02/2010
Days